quaternary

MDPI

Article

A Cryptotephra Layer in Sediments of an Infilled Maar Lake from the Eifel (Germany): First Evidence of Campanian Ignimbrite Ash Airfall in Central Europe

Fiona Schenk [1,*], Ulrich Hambach [2,3], Sarah Britzius [1,4], Daniel Veres [2] and Frank Sirocko [1]

[1] Institute for Geosciences, Johannes Gutenberg University, 55128 Mainz, Germany; sirocko@uni-mainz.de (F.S.)
[2] Romanian Academy, Institute of Speleology, 400006 Cluj-Napoca, Romania; ulrich.hambach@uni-bayreuth.de (U.H.); dan.veres@acad-cj.ro (D.V.)
[3] Bayreuth Center of Ecology and Environmental Research (BayCEER), University of Bayreuth, 95448 Bayreuth, Germany
[4] Department of Isotope Geochemistry, Max Planck Institute for Chemistry, 55128 Mainz, Germany
* Correspondence: fschenk@uni-mainz.de

Abstract: We analyzed mineralogical characteristics, and major as well as rare earth element concentrations, from a cryptotephra layer in sediments of the infilled maar of Auel (Eifel, Germany). The results of detailed geochemical analyses of clinopyroxenes and their glassy rims from the Auel cryptotephra layer showed that they are similar to those from the thick Campanian Ignimbrite tephra occurrence in a loess section at Urluia (Romania). Both tephras show idiomorphic green clinopyroxenes and formation of distorted grains up to millimeter scale. The cryptotephra in the Auel core has a modelled age of around 39,940 yr b2k in the ELSA-20 chronology, almost identical to the latest $^{40}Ar/^{39}Ar$ dates for the Campanian Ignimbrite/Y-5 (CI/Y-5) eruption. These observations suggest that parts of the CI/Y-5 ash cloud were transported also northwestward into Central Europe, whereas the main branch of the CI/Y-5 ash plume was transported from southern Italy towards the NE, E, and SE. Based on pollen analyses, we conclude there was no direct effect on vegetation from the CI/Y-5 fallout in the Eifel area. Trees, shrubs, and grasses remained at pre-tephra-airfall levels for roughly 240 years, but changed around 39,700 yr b2k when thermophilic woody plants (e.g., *Alnus* and *Carpinus*) disappeared and *Artemisia* spread. This change in vegetation was well after the Laschamp geomagnetic excursion and also after the GI9 interstadial and quite probably represents the onset of the Heinrich Event 4 (H4) cold spell, when climatic conditions over the North Atlantic, and apparently also in Central Europe, deteriorated sharply.

Keywords: Eifel maar sediments; Campanian Ignimbrite tephra; Marine Isotope Stage 3; Greenland Interstadial 9; Heinrich Event 4; green clinopyroxene

Citation: Schenk, F.; Hambach, U.; Britzius, S.; Veres, D.; Sirocko, F. A Cryptotephra Layer in Sediments of an Infilled Maar Lake from the Eifel (Germany): First Evidence of Campanian Ignimbrite Ash Airfall in Central Europe. *Quaternary* **2024**, *7*, 17. https://doi.org/10.3390/quat7020017

Academic Editor: James B. Innes

Received: 22 December 2023
Revised: 1 March 2024
Accepted: 15 March 2024
Published: 25 March 2024

1. Introduction

The Eifel is a low mountain range in western Germany, which is characterized by intraplate volcanism [1]. The volcanic Eifel can be divided into three areas: the High Eifel, with volcanic activity from the Tertiary, and the Western and Eastern Eifel, which host the largest Quaternary volcanic fields in Germany, characterized by late Pleistocene maar structures. More than 20 of the Pleistocene infilled maar lakes have been cored by the ELSA (Eifel Laminated Sediment Archive) project at Johannes Gutenberg University Mainz (https://elsa-project.de, accessed on 27 October 2023). For this study, we mainly used the sediments from the infilled maar lake of Auel, which cover the time of the Marine Oxygene Stage 3 entirely [2]. Tephra layers from the Marine Isotope Stage (MIS) 3 Eifel volcanism has been documented by Förster et al. [3]. The search for these tephra produced evidence for a section with volcanic particles at the end of Greenland Interstadial 9 (GI9). These

particles appear not to be from volcanic sources in the Eifel, and they were detected in a stratigraphical interval known for the occurrence of the Campanian Ignimbrite (CI).

The CI ash is a phonolithic to trachytic tuff from a Late Pleistocene volcanic event, apparently the largest eruption during the MIS 3 in Europe (Silleni et al. [4] and references therein). It is derived from the Campi Flegrei in the Campania region (Central Italy) (Figure 1). A huge caldera shapes the landscape of the Campi Flegrei, consisting of a subaerial and a submerged part and covering a total area exceeding 200 km^2. This characteristic structure formed during two major caldera collapses related to the eruptions of the CI/Y-5 during the MIS 3 and the younger Neapolitan Yellow Tuff (NYT) in the late MIS 2 (e.g., Pabst et al. [5]). Fisher and Schmincke [6] described a Plinian character of the eruption, in which gases are transported many kilometers into the atmosphere and can even reach the stratosphere. Fedele et al. [7] calculate the volume of the magma to be at least 200 km^3. Based on a study by Silleni et al. [4], the total erupted bulk volume estimate is now at 457–660 km^3 (181–265 km^3 dry rock equivalent). This volume corresponds to an eruption magnitude of 7.7–7.8 and to a Volcanic Explosivity Index of 7, which makes the eruption the largest in Europe during the Late Pleistocene and probably beyond.

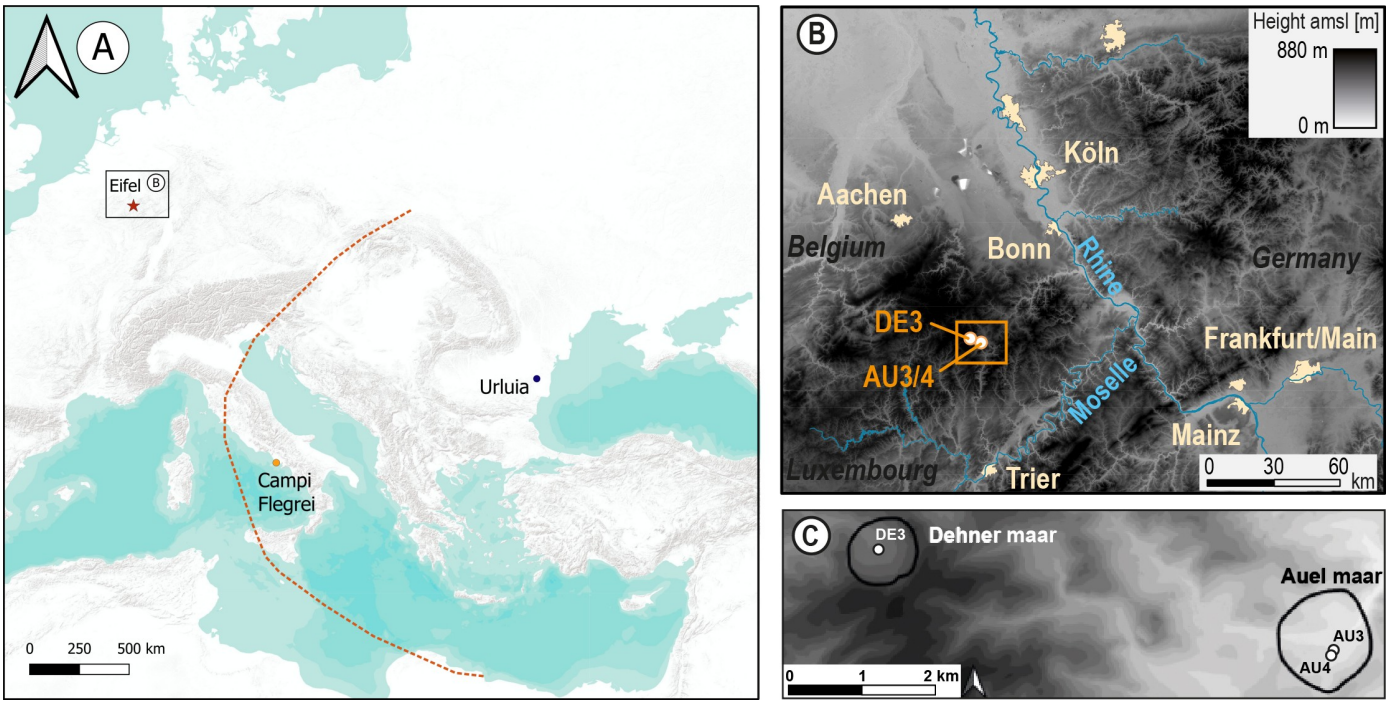

Figure 1. (**A**) Schematic view of the distribution of the CI tephra in Europe (dashed orange line open to the east); Campi Flegrei as eruption site (orange dot; 40.8275° N, 14.1402° E); Urluia as find spot (blue dot; 44.0947° N, 27.9021° E); Eifel Lake sediment cores (red star); scale 1:20,000,000, EPSG: 3857, bounding box: −27,431.587, 3,598,880.852, 4,408,568.450, 7,668,605.656, created with QGIS, base map WorldTerrain by USGS, Esri, TANA, DeLorme, and NPS (Fiona Schenk and Florian Thiery, CC BY 4.0, via https://codeberg.org/ResearchSquirrels/ci-map, accessed on 13 February 2024). (**B**) Eifel (orange-colored marking) and analyzed locations of cores AU3 (50.2825° N, 6.5951° E) and AU4 (50.2821° N, 6.5949° E) in Auel maar and core DE3 (50.2928° N, 6.5066° E) in Dehner maar. (**C**) Marks a closer view of the region of Auel maar cores (AU3, AU4) and Dehner maar core (DE3).

The tephra deposit was first dated in marine sediments of the Mediterranean by oxygen isotope stratigraphy that resulted in an interpolated age of about 38,000 yr BP [8]. ^{40}Ar/^{39}Ar dating by De Vivo [9] shifted the age to 39.28 ± 0.11 ka, and that performed later by Giaccio et al. [10] to 39.85 ± 0.14 ka. Lin et al. [11] attribute the CI to a sulfate spike at 39,915 yr b2k or 39,869 yr b2k, which fits the latest ^{40}Ar/^{39}Ar dates very well. However, no glass shards have been identified so far within the Greenland ice core records.

The CI/Y-5 is accordingly a key temporal marker of Quaternary stratigraphy in Europe [4], including marine records [12,13], terrestrial sequences [14], cave environments [7,15], and lake records [16]. Beside the impressive and landscape-shaping proximal volcanic record, the supra-regional dimension of this eruptive event was first recognized from the widespread tephra records in the marine realm. In their review paper, Keller et al. [17] defined stratigraphic zones to which the tephras from marine sediments of the central and eastern Mediterranean were assigned. They proposed a scheme (from V to Z) in which the tephra which we now know originated from the Campi Flegrei was named Y5 and related to the eruption center of Ischia Island in the Campanian vulcanological province. Proximal to the eruption center, the event left behind mainly cooled pyroclastic flows (ignimbrites) and is therefore also named as such, the CI eruption. However, a more complex record is also found proximally on a scale of at least 100 km around the Campi Flegrei, which begins with a Plinian phase (in turn complex in structure but quantitatively subordinate) and ends with the products of the CI eruption, the CI-phase [18,19]. Distally, only airfall tephra deposits are found in the marine as well as in the continental realm, which in turn can also have a complex stratigraphic structure. Even at distances of 1000 km, the sequence begins with tephra of the Plinian phase and then is abruptly overlaid by products (mostly glass ashes) of the CI, the Campanian co-ignimbrite tephra [20]. The total amount of tephras of the co-ignimbrite phase clearly predominates spatially and thus also quantitatively. It is assumed that the final caldera formation (collapse) as a result of the partial emptying of the magma chamber was responsible for the CI and thus for the proximal pyroclastic flows and the widespread distal tephra [4]. Hence, when looking outside Italy at the products of the CI in a distal stratigraphic archive, we are very probably always dealing with a CI layer dominated by the Campanian co-ignimbrite tephra. Silleni et al. [4] explain that it is difficult to estimate a deposit volume as accurate data may be lacking, e.g., due to the thinning of ash layers, which is essentially the issue. Distal tephras from the CI eruption have been described thus far in Italy, North Africa, over large parts of the eastern European continent as far as Kostenki at the Don River in Russia, in the central and eastern Mediterranean Sea, and in the Black Sea (Figure 1A; for review, see [4,14,21–26]). The CI is widespread in southern Romania and northern Bulgaria, often found in loess–paleosol sequences (LPSs) and in fluvial and cave deposits, and is easily identifiable by the characteristic geochemical fingerprints of the well-preserved glass shards (e.g., Tsanova et al. [27]). It can reach thicknesses from several decimeters up to more than 1 m [24], as is the case for a loess–paleosol section (Figure 2) near the village of Urluia (Romania). The sample used in this study was taken from the base of this ash layer, and optically stimulated luminescence (OSL) dating of the surrounding loess just below the tephra revealed ages ranging from 38.7 $\pm$ 3.3 ka to 41.1 $\pm$ 3.4 ka [24].

The geochemical and mineralogical compositions of the proximal CI/Y-5 volcanic products were analyzed in several studies (Fedele et al. [18] and references therein; [28]). In decreasing order of abundance, minerals of alkali feldspar, plagioclase, clinopyroxene, biotite, magnetite, and apatite are typical phenocrysts of the dominant glassy matrix. Next to the ubiquitous glass, a greenish clinopyroxene (cpx) is characteristic of these deposits. Further analyses can be found in Tomlinson et al. [29] and Civetta et al. [21]. Veres et al. [14], for example, examined glass shards in different locations in Romania (Caciulatesti, Draganesti-Olt, Daneasa, and Lunca). The chemical composition was similar to the values from the CI eruption which were found in the Eifel cores (see Section 3.1.). SiO_2 also dominated there with 58–62 wt% , followed by around 7–10 wt% K_2O and 3.5–7 wt% Na_2O. Traces of CaO and FeO were also present there.

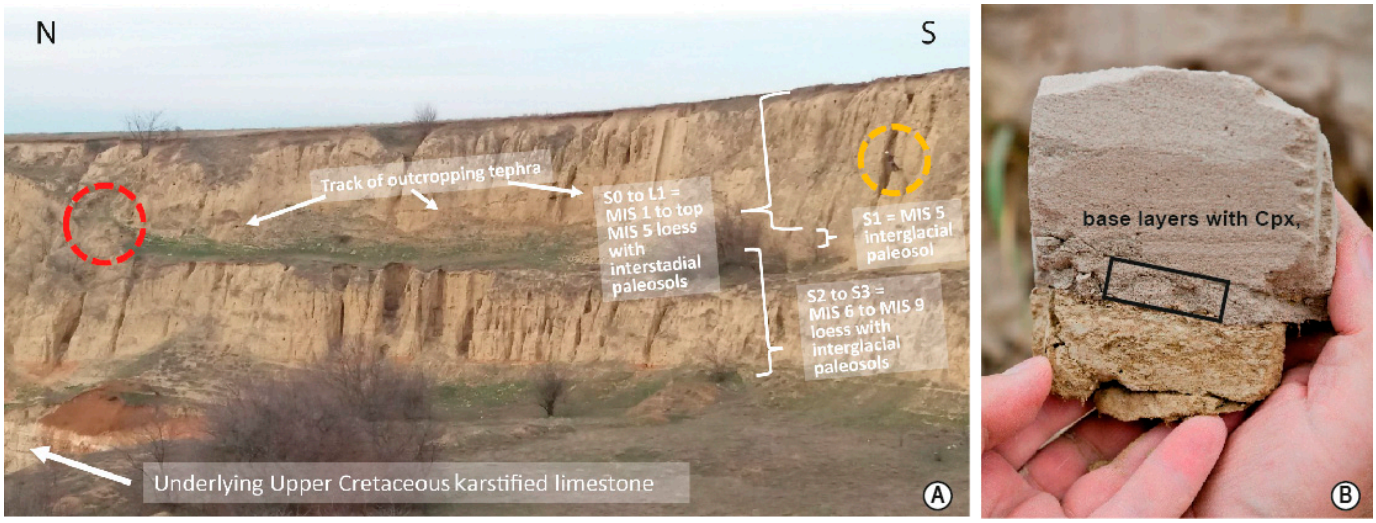

Figure 2. View of the Urluia loess deposit looking east (**A**). The outcrop is an abandoned quarry in which Pleistocene loess discordantly overlies Upper Cretaceous karstified limestone. The entire loess wall is about 800 m long. Its southern 400 m long interval strikes almost exactly S–N, whereas to the north, the wall strikes SE–NW. The outcrop image displays the central part of the outcrop in which the wall changes direction of strike. The height of the loess cliff varies along the wall and measures in average between 15 and 25 m and represents in its upper part the last glacial cycle (MIS 1 to MIS 5; compare to Figure 3 in Fitzsimmons et al. [24] and Figure 3 in Obreht et al. [30]). The yellow circle marks a person on ropes sampling loess. The red circle shows the area at which the sample was taken from the base of the tephra layer, which is at this location about one meter thick. Laterally, the tephra thins out towards the south and north, eventually appearing as cryptotephra mixed up with loess but still recognizable. Part (**B**) displays a sample from the base layer of the tephra in direct contact with the underlying loess—similar to that used in this study (beige sediment held by left hand = loess, and greyish material with sandy appearance = tephra; black frame indicates the analyzed basal layer). For Pleistocene loess stratigraphy, we refer to Marković et al. [31].

Prior to this study, no possible CI tephra had been reported in Central Europe. Either the CI plume did not reach that far north or west, or it had not been observed due to the lack of high-resolution MIS 3 records in Central Europe. Most MIS 3 lake basins in Northern Europe were overrun by the glaciers of the Last Glacial Maximum (LGM), and lakes in the Alpine foreland by mountain glaciers and their meltwater runoff. However, the so-called Neapolitan Yellow Tuff (NYT), a late glacial tephra layer stemming from the same eruption center and dated to 14.9 ka, was recognized in Lake Längsee in the southeastern Alps (Austria) [32,33]. This finding indicates that there are atmospheric circulation patterns through which volcanic ash such as NYT could be transported directly northwards from the Campi Flegrei towards Central Europe.

2. Materials and Methods

2.1. Samples

The samples investigated in this study were taken from drill cores of infilled maar lakes from the Eifel region (Germany) and from the Urluia loess sequence on the Dobrogea Plateau in SE Romania close to the Black Sea. The Romanian site was chosen for comparison because, as with the cryptotephra found in the Eifel, it represents a distal occurrence of the CI. In Urluia, however, there is a thick and unworked tephra deposit of exceptional thickness. The drill cores AU3 and AU4 are from the infilled maar lake at Auel (Eifel, Germany) and the drill core DE3 is from the Dehner infilled maar (Figure 1B,C). Photos of the respective core sections are shown in Figure 3. The Auel cores were used to construct the ELSA-20 chronology [2], which is the basis for the dating of the CI as described later in this paper. The AU3 core has a length of 102 m and coordinates of 50.2825° N and 6.5951° E

(456 m above sea level) while AU4 has a length of 104.50 m and coordinates of 50.2821° N and 6.5949° E (457 m above sea level). The Eifel area at the Dehner maar, whose drill cores provide a comparison, is 100 m higher. The DE3 core (50.2928° N and 6.5066° E) has a length of 88 m and was located at 565.37 m above sea level. The CI tephra is not visible to the naked eye in any of these three drill cores, which is why it is referred to as cryptotephra.

The sample at Urluia (southeastern Romania) was taken from the Dobrogea Plateau separating the Lower Danube steppe landscape from the Black Sea. The CI layer is found in the upper part of a loess package stratigraphically ranging from the Middle Pleistocene (≥MIS 11) to the Holocene (44.0947° N, 27.9021° E) and situated at about 110 m above sea level [30]. We described the analysis from a scatter sample of the tephra from Urluia in more detail (cf. Section 3.1).

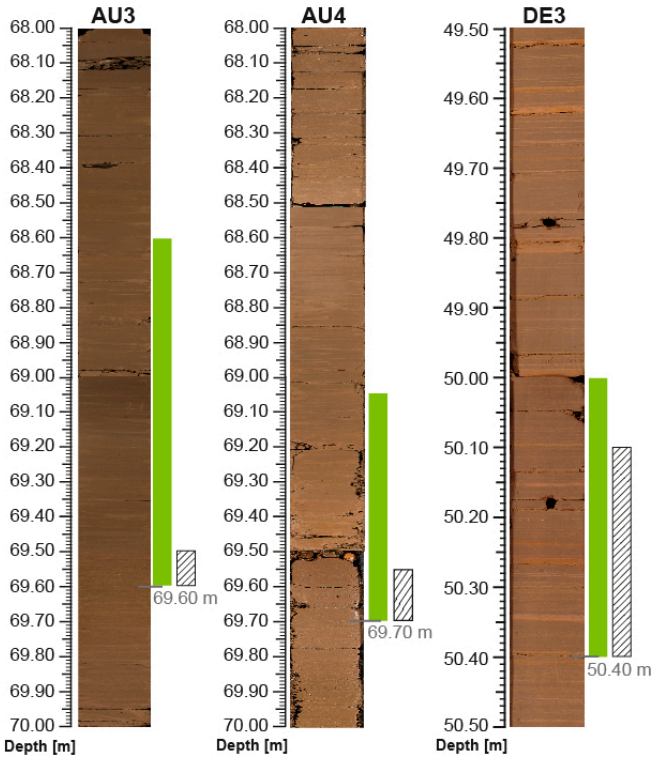

Figure 3. Photographs of lake sediment cores from Auel maar and Dehner maar (green markings define presence of cpx, dashed markings show distorted grains). The age in these selected parts was determined to be about 40,000 to 39,000 yr b2k (Sirocko et al., unpublished).

2.2. Optical Analysis

Mineral grains in the dried fraction >150 µm were analyzed under a binocular (M3Z binocular from WILD, Heerbrugg, Switzerland) with a zoom range of 6.5×–40×. The samples of AU3, AU4, and DE3 were analyzed in 10 cm increments.

The optical analysis was used to screen the entire sand fraction of the mineral grains, but in particular greenish clinopyroxenes (cpxs) and distorted grains were counted. Greenish cpx can occasionally appear in Eifel tephra deposits [34], but the distorted grains appear to be unique and have not been documented for any of the other tephra in the ELSA cores; see Sirocko et al. [1]. Cpxs generally occur as euhedral to subhedral crystals (up to 1 mm in size) with a homogeneous pale green color, suggesting textural equilibration with the host glass [35]. The distorted grains reflect mechanical stress in their plastic state. Following Kendrick [36], the distorted grains are the results of deformation at the viscous–brittle transition in magma during its ascent. At this transition, phenocrysts experience brittle deformation and, in the intact segments, crystal-plastic deformation. This process apparently involved several quite different particles but showed the same habit in Auel and Urluia. To further document that these minerals are indeed from the same eruptive

source, we analyzed the geochemistry of greenish cpxs in both the Eifel cores and the Urluia sample (Figure 4).

2.3. In Situ Reflectance Spectroscopy (ISRS, C_{org}(chlorins))

The method was described by Sirocko et al. [2] for the two Auel cores. The ISRS670 was determined with a Gretag spectrolino that measures sediment reflection. The sediment surface in the core scan was an integration of a 2.5 mm wide area, and the individual measurements were taken in 1 mm increments. The light absorption at 670 nm (ISRS670) was caused by chlorophyll derivates from the organic matter of diatom and chrysophytes; the absorption data are presented from cores AU3 and AU4 as C_{org}(chlorins) versus age and versus depth (Section 3.2), which allows detection of GI8 and GI9. The entire sediment section between these interstadials was analyzed for the occurrence of greenish cpxs, which occur together with distorted grains in both Auel cores (AU4, AU3) as well as in core DE3 of the Dehner maar.

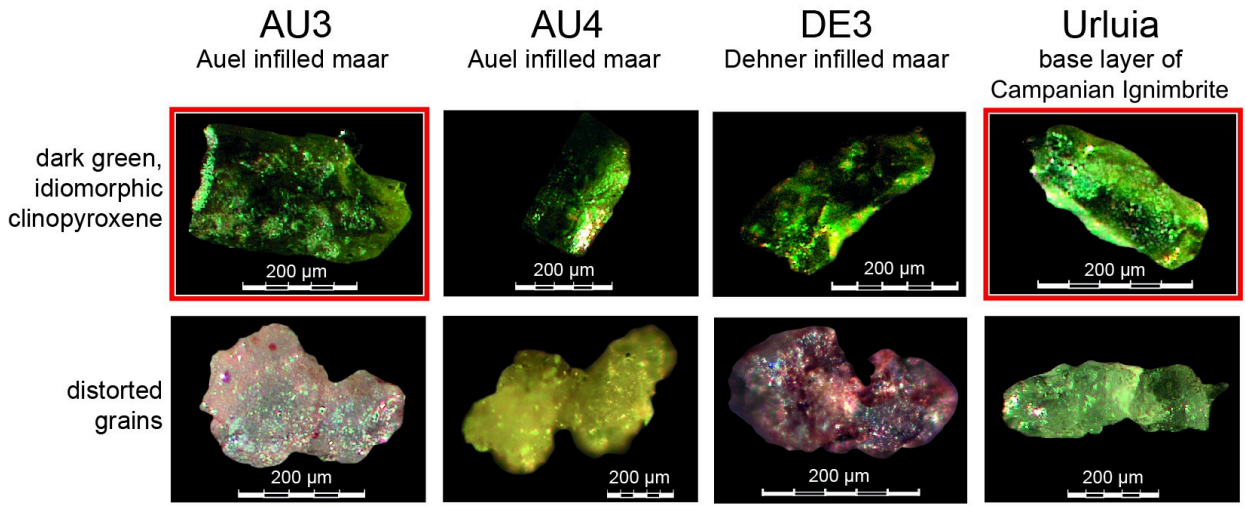

Figure 4. Overview of minerals in stratigraphically corresponding depths [m] of the Eifel drill cores of Auel maar and Dehner maar (Germany) as well as in the loess deposit at Urluia (Romania). The red-marked pictures indicate the cpx samples used for geochemical analysis (EPMA and LA-ICP-MS, see Section 3.1).

2.4. Geochemistry

Geochemical analyses were carried out at the Institute for Geosciences of Johannes Gutenberg University (Mainz), the Bavarian Geoinstitute Bayreuth (BGI, campus of the University of Bayreuth), and at the Max Planck Institute for Chemistry in Mainz.

Electron probe microanalysis (EPMA) and laser ablation–inductively coupled plasma–mass spectrometry (LA-ICP-MS) were performed in Mainz and Bayreuth. At Mainz, one dark green, idiomorphic cpx from the AU3 core and one from the Urluia sample were selected for EPMA (Figure 4, red-marked picture). The preparation of the cpx samples and EPMA were carried out according to the method of Reed [37] using a Leica DMRX point logger (objective: PL Fluotar 5×/0.12P ∞/-/B) which was equipped with an automatic X,Y stage. Overall, 20 EPMA readings were carried out, 14 on the AU3 and 5 on Urluia green cpxs.

Trace element analysis for rare earth elements (REEs) was performed using LA-ICP-MS according to Prelević et al. [38]. The analysis of the elements was carried out using an Agilent 7500ce ICP-MS coupled to a NewWave NWR 193 (ArF Excimer Laser 193). After EPMA, two uniform green cpxs were selected for this analysis, one from the AU3 core (EPMA sample 10) from the Eifel region (Germany) and the other (EPMA sample 14) from the loess deposit in Urluia. For this purpose, laser ablation (LA) was first performed on the surface of the cpxs. With the formation of a plasma, the minerals heated up so that they

were detected and subsequently ablated. After this, the cpxs were transported with argon into the inductively coupled plasma (ICP) ion source of a corresponding mass spectrometry (MS), in which they were evaporated in hot plasma, atomized, and positively ionized, and then they were transferred to the high vacuum of a mass spectrometer.

At the Bavarian Geoinstitute Bayreuth, for EPMA of the cpx minerals, including attached glassy rims, carefully picked minerals were mounted in epoxy resin, ground, and polished. Major oxide chemical compositions of the oxides were determined using single-grain, wavelength-dispersive electron microprobe analysis on a Jeol JXA8200 microprobe employing an accelerating voltage of 15 keV, a 6 nA beam current, and defocused beam. The order of measured elements (first to last) was as follows: Na, Si, K, Ca, Fe, Mg, Al, P, Ti, Mn, Cl, with peak counting times averaging 10 s for Na, 30 s for Si, Al, K, Ca, Fe, and Mg, 40 s for Ti and Mn, and 60 s for P. Precision was estimated at <1–6% (2σ) and 10–25% (2σ) for major and minor element concentrations, respectively.

The LA-ICP-MS system at BGI consisted of an Elan DRC-e quadrupole mass spectrometer (Perkin Elmer Instruments, Vaughan, ON, Canada) attached to a Geolas M 193 nm ArF Excimer Laser system (Coherent Inc., Saxonburg, PA, USA). Technical details about this system can be found in Günther et al. [39]. Pyroxene was ablated using a laser beam of 40 µm in diameter. The laser was operated at a frequency of 10 Hz and an output energy of 80 mJ, which results in an energy density of ca. 10 J/cm^2 at the sample surface. The sample chamber was flushed with helium gas at a rate of 0.4 l/min, to which Ar was added on the way to the ICP-MS. Instrument background was measured for 30 s before each analysis, and the sample was measured for another 30 s. The masses Na^{23}, Mg^{25}, Al^{27}, Si^{29}, P^{31}, K^{39}, Ca^{42}, Sc^{45}, Ti^{49}, V^{51}, Mn^{55}, Fe^{57}, Rb^{85}, Y^{89}, Zr^{90}, Nb^{93}, Cs^{133}, Ba^{137}, La^{139}, and Ce^{140} were measured with a dwell time of 10 ms, whereas V^{51}, Sm^{147}, Dy^{163}, Er^{167}, Lu^{175}, and Ta^{181} were measured with a dwell time of 20 ms. Integrated signal intensities were referenced to NIST SRM 610 glass [40] according to routines described in Longerich et al. [41]. Calculated element ratios were then turned into absolute values by normalizing all major and minor element oxides to 100 wt%.

Furthermore, spatially high-resolution major element analyses on core halves were performed with an Avaatech X-ray fluorescence core scanner at the Max Planck Institute for Chemistry in Mainz. The method is described in Richter et al. [42].

2.5. Pollen

The pollen sample preparation was carried out according to Berglund and Ralska-Jasiewiczowa [43] and Fægri and Iversen [44]. The long pollen sequences for the Auel cores were presented in detail by Britzius et al. [45].

3. Results

Green clinopyroxenes (cpxs) as well as the distorted grains were observed in the base layer of the CI tephra at Urluia (Figure 4), and also in the Eifel cores in the sediment section subsequent to GI9. The optical analysis of sediments in the cores of the Auel maar revealed green cpxs at depths of 68.60–69.60 m in AU3, and 69.05–69.70 m in AU4. The base of these depths corresponds to an age of about 39,850 ± 150 yr b2k in the ELSA-20 chronology [2]. Distorted grains were detected in AU3 at 69.50–69.60 m, and 69.55–69.70 m in AU4. In addition, the green cpxs from both Auel cores and Urluia show frequently a glassy rim. The results of the EPMA showed an almost identical composition to the CI glasses known from proximal CI and distal tephra deposits [14,18].

Apparently, the distorted grains are exclusively associated with the first phase of the eruption. Furthermore, Kendrick et al. [46] pointed out that shear forces occur in the conduit during the eruption process deforming minerals in the crystal mash, particularly with the type of magma from which the CI originated. On the one hand, this may lead to fracturing, but also to plastic deformation depending on the physical state of the magma in the eruption conduit (viscous, plastic, brittle) [36,46]. Distorted grains have been analyzed in detail by Okumura et al. [47], and for further reading about these known phenomena, see also the

work by Holness et al. [48]. X-ray images clearly indicated the "twisted form" of distorted grains. In addition, Arbaret et al. [49] presented the results of deformation experiments of melts produced in the laboratory, in which fractured deformation of minerals occurs, producing seemingly distorted grains. Further investigations are necessary to clarify the process which leads to the formation of the distorted grains found in our samples.

Figure 5 shows the titanium (Ti), potassium (K), and vanadium (V) contents in the Eifel drill cores AU4 and DE3, normalized to aluminum (Al). The stratigraphic record in these Eifel drill cores reveals increased element ratios of Ti/Al, K/Al, and V/Al indicative of cryptotephra occurrence (e.g., Tomlinson et al. [29]). Vanadium was unfortunately not measured in the DE3 core. Apparently, cpxs and distorted grains occur in a section with higher values of Ti/Al and K/Al.

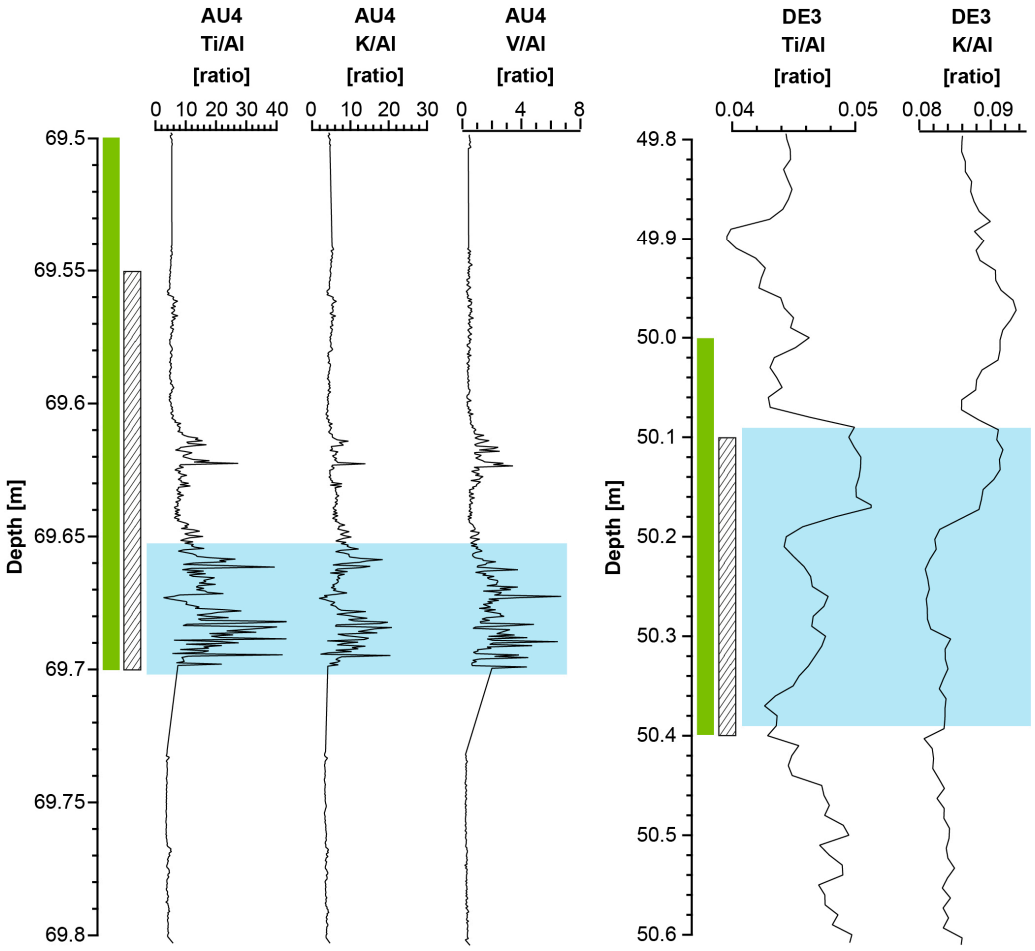

Figure 5. Element ratios in the Eifel drill cores AU4 and DE3 indicative of cryptotephra occurrence (blue area = increase and field of the higher values of the chemical ratios; green strip = green cpxs; dashed strip = distorted grains). The values for the AU4 core are from Sirocko et al. [2].

3.1. Geochemical Analysis

The results of EPMA (Figure 6A) and LA-ICP-MS (Figure 6B) on green cpxs from the AU3 core (depth of 69.50–69.60 m) and Urluia demonstrate a comparable distribution of main elements and a similar rare earth element spectrum. Both samples contain about 50% SiO_2 as well as high CaO (>20%) and MgO (>10%) values. Additionally, FeO and Al_2O_3 were found in both samples with slightly different values of about 8% for FeO and Al_2O_3 in the Eifel cpxs and 10% (FeO) and only 3% (Al_2O_3) in the cpxs from Urluia. The chemical compositions of the glassy rims show that the glasses also have a high proportion of SiO_2 (60.01%). However, it is noticeable that the glass also contains relatively high Na_2O, K_2O, CaO, and MgO contents. This suggests that cpxs with glassy rims do not originate from

the Eifel region, as tephra from the Eifel were relatively low especially in K_2O, CaO, and MgO while SiO_2 approached 60%. The only tephra with a similar geochemical composition investigated by Förster et al. [3] was a tephra from the Hoher List maar (HL4, 42.20 m), which was, however, older than 100 ka. The obtained values were confirmed by Wulf et al. [50] in presenting and discussing geochemical data for volcanic glass from tephras in lake records from northern Greece. Furthermore, the chemical compositions from the CI samples in Auel and Urluia differ significantly from the data for cpxs and glass from tephras originated in the Eifel region slightly older than 40 ka (Dreiser Weiher, Meerfelder Maar) [3]. ‘

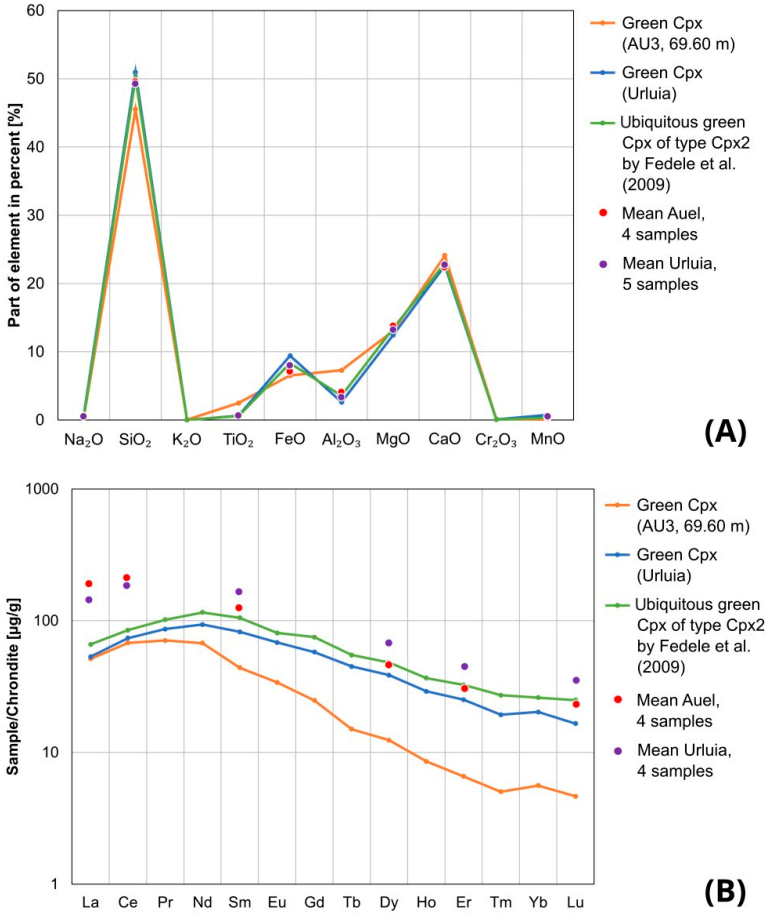

Figure 6. Major element (EPMA, (**A**)) and trace element (LA-ICP-MS, (**B**)) contents of cpxs from Auel and Urluia. Two green cpxs (sample 10 from core AU3, orange line; sample 14 from Urluia, blue line) were analyzed at the Institute for Geosciences of the Johannes Gutenberg University, Mainz. The mean values of the measurements of 4 cpxs each from Auel (red) and Urluia (purple) were analyzed at the Bavarian Geoinstitute Bayreuth (BGI, campus of the University of Bayreuth). The EPMA values are compared with the data of Fedele et al. [35] (green line). The LA-ICP-MS data are normalized to chondrites using data from Evensen et al. [51].

The major elements compositions of cpxs and glass presented in Figure 6A as well as in Appendix A (Table A4, and in Tables A1 and A2a,b), show the overall good agreement of the chemical compositions obtained from Auel (AU), Urluia, and the Campi Flegrei. For the latter, compositional data of glass from the most voluminous Welded Grey Ignimbrite (WGI) from the study of Fedele et al. [18] were selected. Moreover, for the glass data, the average was only calculated from samples for which all elemental analyses were above the detection limit (38 data sets). Despite increasing relative differences with decreasing absolute element concentrations, the compositions lie within the known variation range of the CI eruption products and thus suggest a common origin of minerals and glass.

In Figure 6B and Table A3, average rare earth element (REE) compositions of cpxs (LA-ICP-MS data) for samples from the Breccia Museo Formation (Campi Flegrei; e.g., Fedele et al. [52]) are shown in comparison to results obtained for cpxs from the Auel cores and Urluia. The Breccia Museo Formation was interpreted as a proximal facies of the CI eruption products. The Cpx2-type clinopyroxenes of this sample set are most widespread in trachytes and less abundant in trachyphonolites and therefore originated from a less evolved trachytic magma [35].

The pattern of relative trace element concentrations of green cpx are comparable in both samples (AU3 and Urluia) in the entire REE spectrum (Figure 6B and Table A5) with slightly lower element concentrations in the green cpxs from AU3 (Eifel). In both cpx samples, 14 rare elements were detected with the highest concentrations (µg/g) of Nd (≈100 in Urluia/90 in the Eifel), Pr (90/80), Sm (90/70), Ce (80/80), Eu (80/60), La (70/70), and Gd (75/50), and decreasing content values for trace elements Tb, Dy, Ho, Er, Tm, Yb, and Lu with up to 25 µg/g (Urluia) and 8 µg/g (AU3).

Green cpxs from both drill cores of Auel (AU3 and AU4) and from Urluia frequently show a glassy rim, which represents a sample of the magma at the moment of eruption. The results of the EPMA showed an almost identical composition to the CI glasses known from proximal CI and distal tephra deposits [14,18,29,30]. A back scatter electron (BSE) image of a cpx with glassy rim from AU4 and respective EPMA data are shown in Figure 7C.

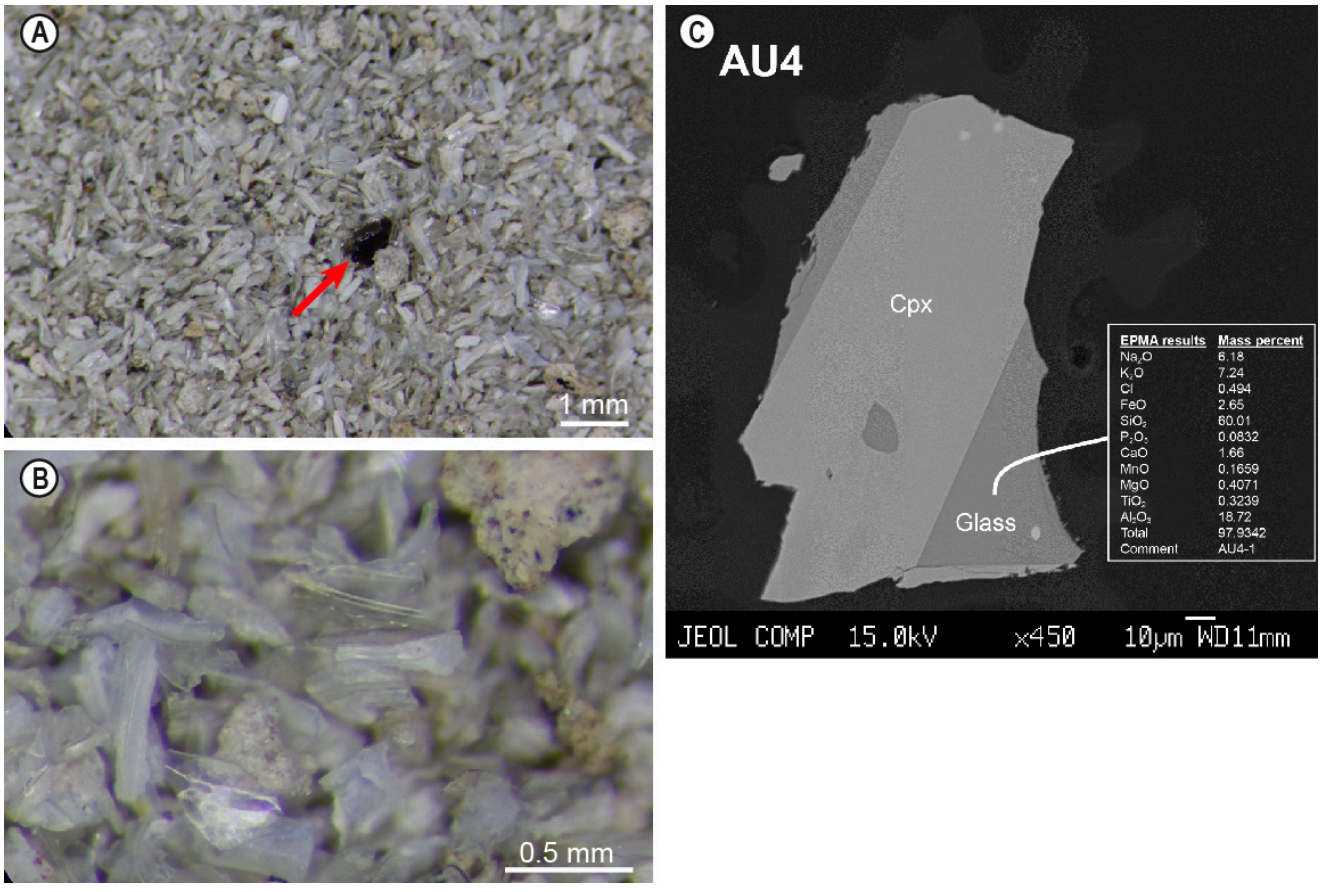

Figure 7. Incident light images of a scatter sample of the tephra from Urluia; only particles larger than 125 µm are shown. In Part (**A**), the red arrow points to a dark green cpx imbedded in glass shards and pumice fragments. The photo of Part (**B**) was taken with 60× magnification, showing glass shards and pumice; the latter is rich in Fe-Ti-oxides (black inclusions) (photos by Philipp Schulte, RWTH Aachen University). Part (**C**) shows a BSE image of a cpx with glassy rim from drill core AU4 including EPMA results for the glass.

3.2. Stratigraphy

The stratigraphy for the subsequently drilled Auel cores AU3 and AU4 was analyzed in 1 mm steps and revealed all Greenland interstadials [2]. The C_{org}(chlorins) records of AU3 and AU4 are plotted in Figure 8 in comparison to the oxygen isotope ($\delta^{18}O$) from the North Greenland Ice Core Project (NGRIP). The C_{org}(chlorins) maxima in the interstadial around GI9, and thus corresponding to the timing of the CI eruption, are well detectable. Figure 9 shows the intervals of the Auel cores (AU4, AU3) and Dehner core (DE3) where greenish cpxs and distorted grains were visible in the sieved fraction > 150 µm. The distorted grains were concentrated in a small section, which we interpreted to be the base of the CI fallout.

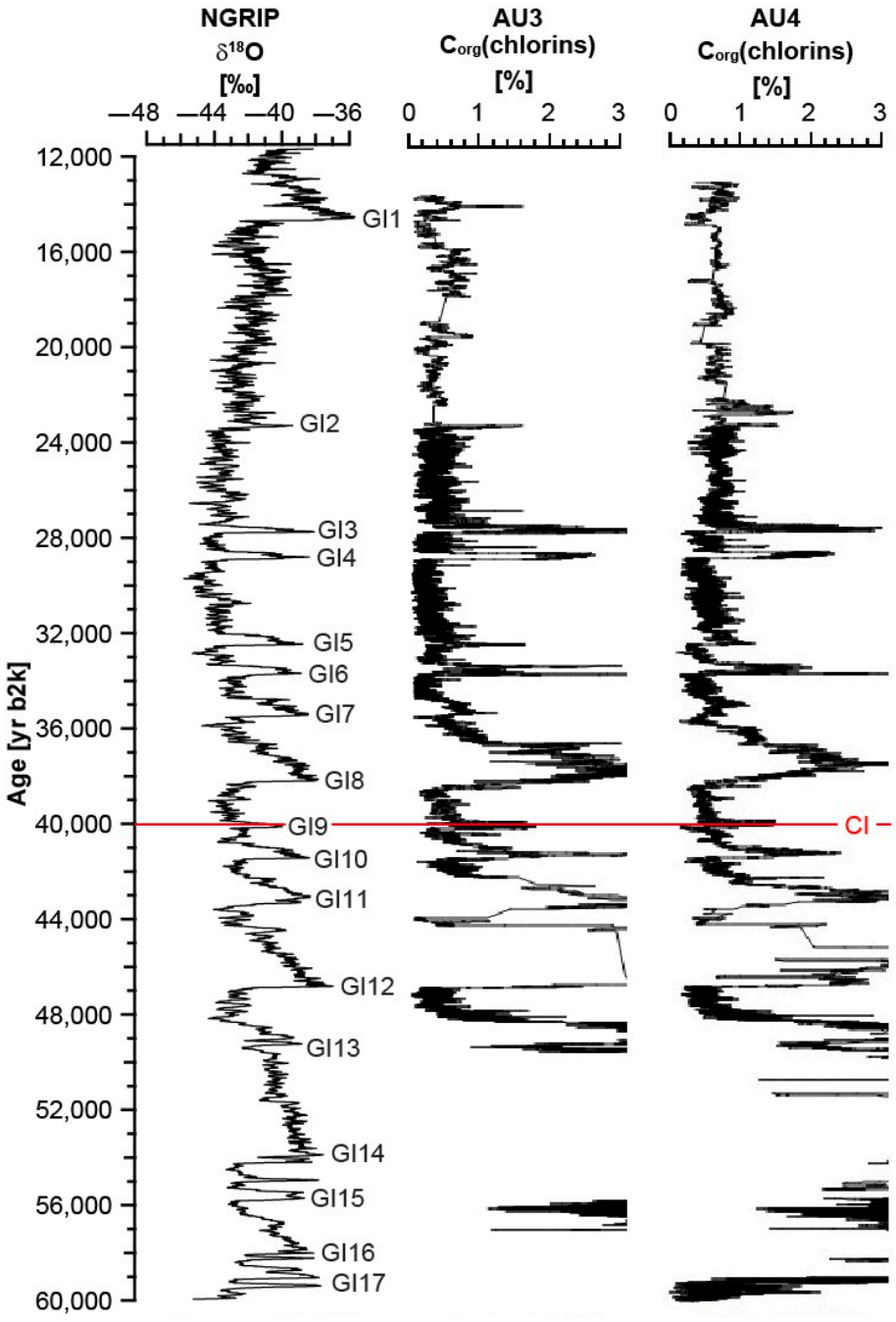

Figure 8. ELSA data (C_{org}(chlorins)) from Auel maar (AU3, AU4) [2] in comparison to the NGRIP ($\delta^{18}O$) [53]. C_{org}(chlorins) data were smoothed with a 12 pt mean and $\delta^{18}O$ with a 40 pt running mean. The position of the CI layer is marked as a red line.

The positions of greenish cpxs and distorted grains in AU3 are very close, but not exactly at the same position within the GI9 C_{org} maximum. This can be explained by bioturbation of the sediments in both cores AU3 and AU4. Micro-bioturbation by chironomids reaches only mm-cm, whereas bioturbation by fish reaches cm-dm. We also cannot exclude the possibility that the deposition of the K-rich glass resulted in a change in water nutrient content, or even diagenetic processes. Further investigations of the detailed structure of the CI fallout layer is planned for other ELSA cores, which potentially document GI9 in varved quality, which is not case for AU3, AU4, and DE3.

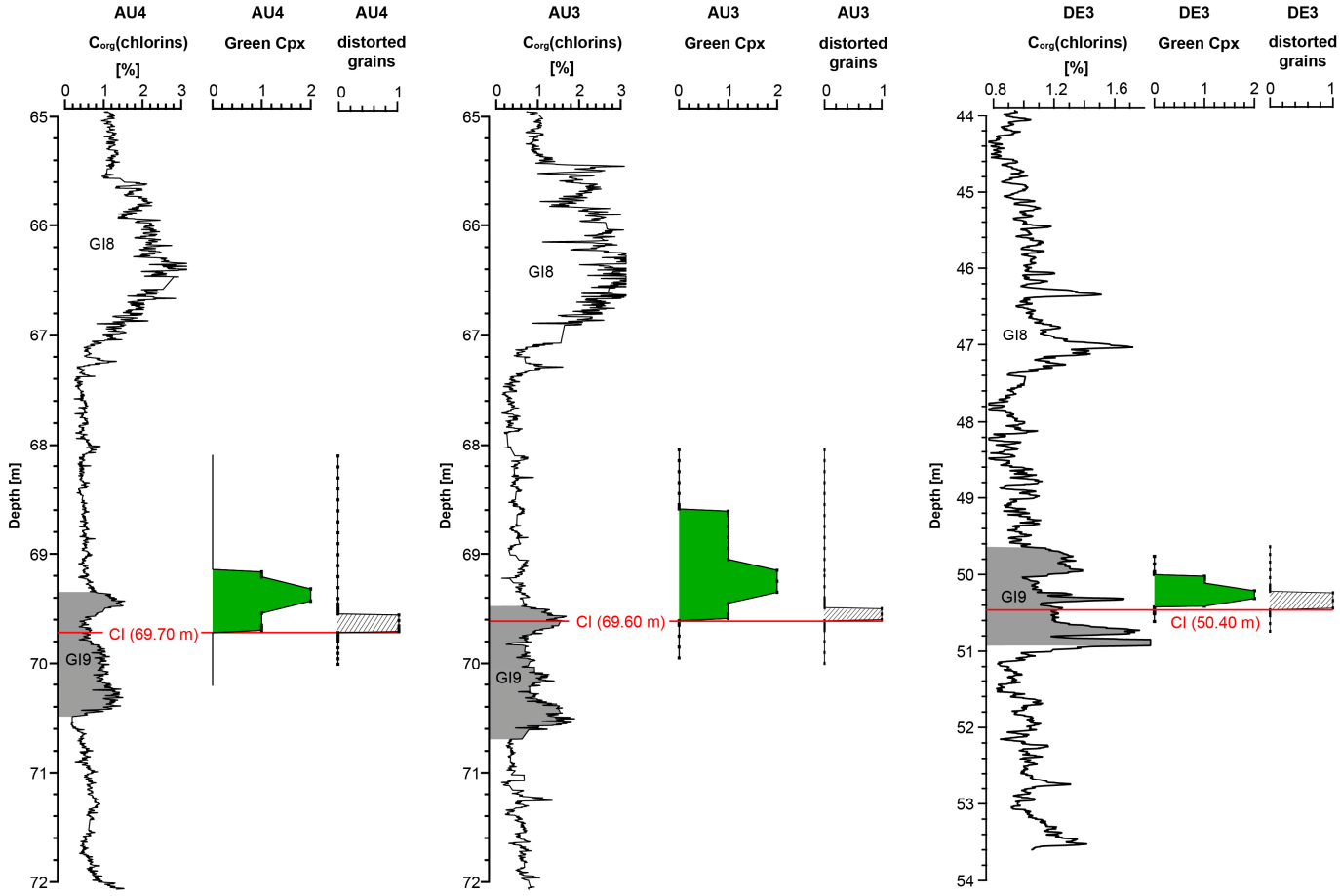

Figure 9. ELSA data (C_{org}(chlorins) of drill cores taken from Sirocko et al. [2], occurrence of cpxs and distorted grains) in Auel maar and Dehner maar against depth [m]. Cpx is marked as a green area (numbers define quantity). Locations of the distorted grains are indicated in dashed markings (numbers define presence). C_{org}(chlorins) data were smoothed with a 5 pt running mean. CI is marked as a reddish line.

3.3. Result Summary

The results above have documented the depth of a cryptotephra layer linked here with the CI at 68.60–69.60 m in core AU3, 69.05–69.70 m in AU4, and 50.00–50.40 m in DE3. The first appearance of distorted grains in the ELSA-20 chronology appears to be the most probable depth representing the initial CI fallout in the Eifel area. The characteristics and curves of Figures 3–9 repeatedly show the CI before the end of GI9, and thus in the time interval of 39,900–39,950 yr b2k, which is the time window also dated by $^{40}Ar/^{39}Ar$ dating [9,10]. The CI in AU4 was located within a C_{org}(chlorins) minimum in the later phase of GI9, which lasted from 40,160–39,900 ± 150 a b2k [53]. Interpolating the span between the beginning and the end of GI9 in AU4, we propose an age of 39,950 ± 150 yr b2k for the fallout of the CI particles; the error for this age is taken from Rasmussen et al. [53].

4. Discussion

The geochemical and mineralogical compositions of the CI ash which reached Central Europe allow inferences about the dynamics of the cloud transport. This is, however, a topic which needs much more detailed geochemical and isotopic analysis, which we are planning to undertake in a future study. In this paper and in a special issue of *Quaternary* about MIS 3 climate and vegetation, we will finally evaluate if, or what, environmental changes were associated with the CI fallout in Central Europe. The second part of this discussion will then deal with the timing of the eruption relative to global processes, in particular, insolation, paleomagnetism, and North Atlantic hydrographic changes.

4.1. Environmental Change Associated with the Campanian Ignimbrite/Y-5–tephra

Figures 10 and 11 document that pollen in the decades before the CI were the same as during GI9. Boreal tree taxa (*Picea*, *Pinus*, and *Betula*; cf. Figure 11) as well as pollen of Poaceae are dominant throughout the total 68.00–72.00 m depth range; temperate taxa build up to about 20% of the total terrestrial pollen sum from 70.80 to 70.30 m and 69.40 to 68.90 m. These derived mainly from typical trees of the flood plains like *Alnus* and *Salix*, but also *Quercus* (Figure 10). All taxa continued to be present in the decades after the CI; thus, we infer that the environmental change caused by the eruption and deposition of small amounts of ash particles was minimal in the Eifel region.

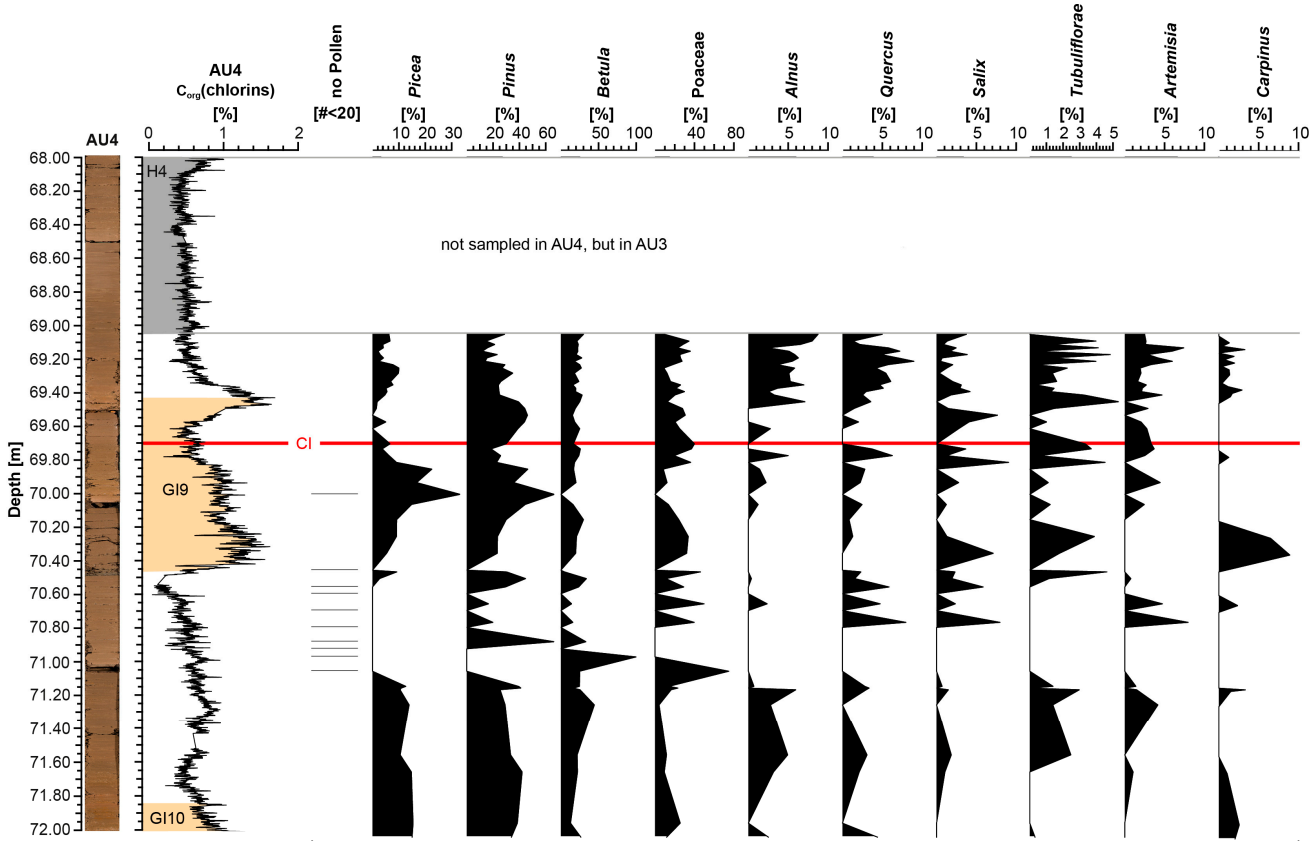

Figure 10. Changes in pollen composition in AU4 (for total pollen sequence of the Auel core, see Britzius et al. [45]) before, during, and after CI layer, compared to C_{org}(chlorins) [2] against depth [m]. C_{org}(chlorins) data were smoothed with a 10 pt running mean. Pollen are shown as the percentages of the total terrestrial pollen sum. No pollen shows the samples where there were only very few pollen preserved and thus less than 20 grains counted.

Tree pollen and C_{org}(chlorins) show two peaks during GI9, one before the CI layer with a duration of about 100 years, and one directly after the CI event. The pollen do not indicate any noticeable change in the vegetation following the CI eruption.

A pronounced change is, however, observed at about 39,700 yr b2k, and thus about 240 years after the CI eruption according to the ELSA-20 chronology. At this time, Poaceae, *Alnus*, *Quercus*, and *Salix* decrease strongly or even disappear from the pollen spectrum. Instead, *Artemisia* spread. This pattern could indeed have been caused by a climate deterioration contemporaneous with the onset of the Heinrich Event 4 (H4) cold spell in the North Atlantic. A precise date for the H4 onset could not be derived from the marine sediment itself; it is thus our ELSA AU4 record which suggests that the onset of H4 was between 39,900 and 39,700 yr b2k, which is consistent with the results of Rasmussen et al. [53]. The CI was thus not directly associated with the onset of the H4 event.

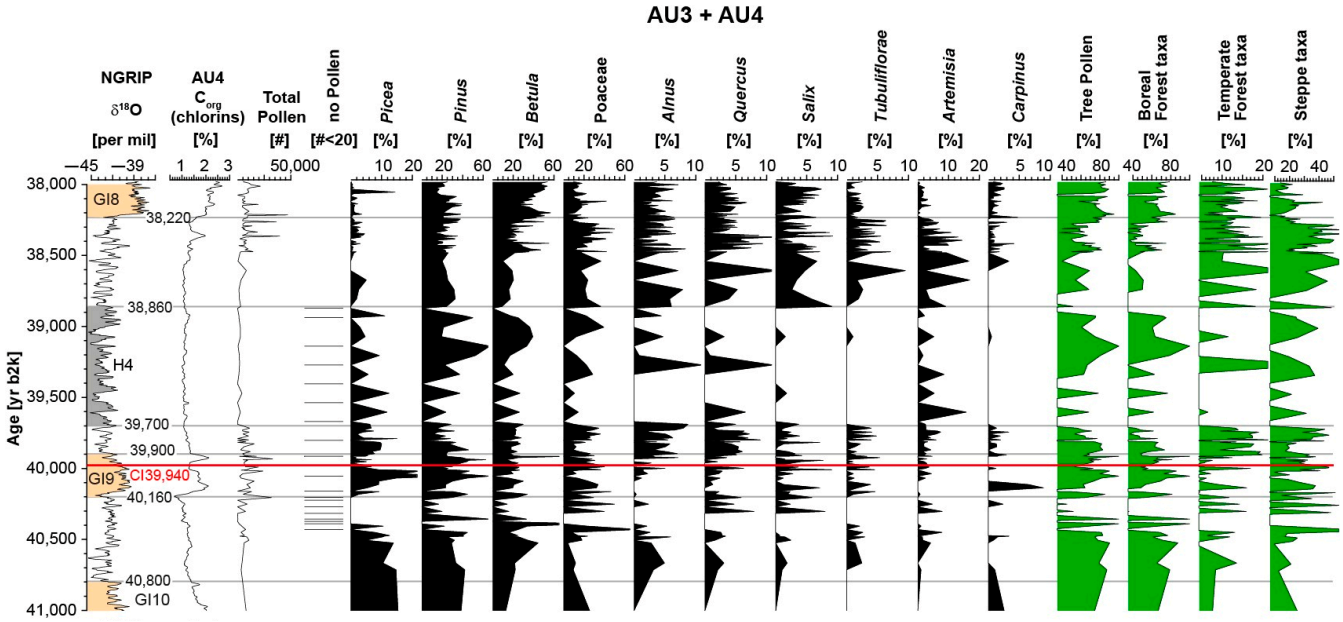

Figure 11. Changes in pollen percentages in AU3 and AU4 (for total pollen sequence, see Britzius et al. [45]) before, during, and after CI layer, compared to C_{org}(chlorins) [2] against age [yr b2k]. C_{org}(chlorins) data were smoothed with a 5 pt and $\delta^{18}O$ data [53] with a 10 pt running mean. Pollen are shown as the percentages of the total terrestrial pollen sum. No pollen indicates the samples where there were only very few pollen preserved and thus less than 20 grains counted.

The CI tephra might have also changed the soil properties in the Eifel volcanic landscape. The decades immediately after the CI show an increase in *Quercus* and *Alnus*, which resulted in an increase in the Temperate Forest summary curve (Figure 11). This increase in temperate taxa during the transition into a cold stadial was unexpected. Thus, we infer that oak and elm might have benefitted from the potassium (K) leached from the ash deposits. The increase in these two trees was paralleled by a C_{org}(chlorins) maximum, one of the very few which are not paralleled by a maximum in the Greenland $\delta^{18}O$. Thus, the C_{org}(chlorins) maximum subsequent to the CI layer could have been caused by an increase in silicium and potassium in the river water, draining the catchment of Auel. This pattern could indeed be attributed to the CI airfall, resulting in the spread of oak and elm trees via K fertilization, the seasonal decay of leaves producing nitrate and phosphate, causing increases in nutrient runoff into the lake system. This must not be the only possible interpretation for the environmental change after the GI, but it would explain all the observed features in the vegetation and the lake C_{org}(chlorins) content.

4.2. Comparison to the Global Climate between 45,000 and 35,000 yr b2k

Massive volcanic eruptions with S-rich ashes reaching the stratosphere are known to potentially effect the climate on a global scale; see the recent example of Pinatubo in 1991 that cooled the Earth temperature for about two years. Costa et al. [54] confirm that the

injection of such aerosols into the stratosphere can lead to an extended volcanic winter. The CI eruption, however, was not as effective. It was difficult to detect the fingerprint of the CI in the Greenland ice at all, and the results of this study show no immediate climate reaction to the fallout event.

Figure 12 presents several records of globally important climate related curves. The geomagnetic intensity, with its pronounced minimum during the Laschamp event, centered at 40,850 yr b2k, was already increasing for several centuries. The H4 events, representing the decay of the North American ice sheet, started with the CI in the marine curve of Martrat et al. [55]. The time resolution of the marine record is not, however, sufficient to resolve this event even with century resolution. The pollen of AU3 presented above indicated that the environment in the Eifel remained stable for 240 years even after the CI event.

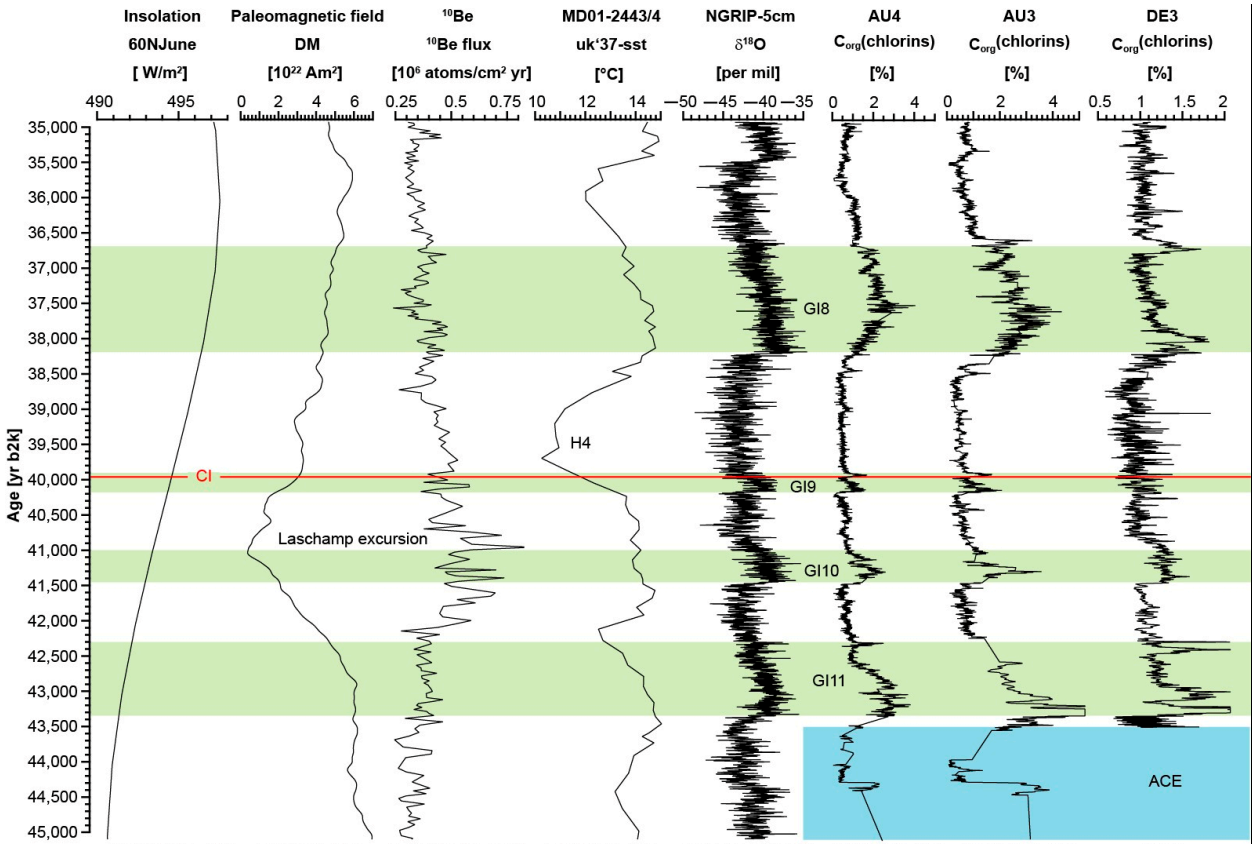

Figure 12. Comparison with global analyses contemporaneous to the timing of the CI [yr b2k]. The ages of the NGRIP and the additional events (GI9, GI8, as well as H4) are based on Rasmussen et al. [53]. Since all events take a certain period of time, the onset is shown here in each case. It also can be seen that the CI occurs after the interstadial period GI9, and coincides with the onset of H4, a cold stadial. $\delta^{18}O$ is smoothed with a 10 pt mean. Berger and Loutre [56] measured insolation at 60° N, the values from SST are from Martrat et al. [55]. Korte et al. [57] provide a global intensity model of the Laschamp geomagnetic surface field expression (the time center of the Laschamp excursion is marked here at 40,850 yr b2k), and Muscheler et al. [58] give the ^{10}Be concentration from ice cores as proxy for the geomagnetic field strength. The comparison to the C_{org}(chlorins) values of AU4 and AU3 cores is from Sirocko et al. [2]. ACE means Auel Cooling Event (compare Albert and Sirocko [59]). ACE (blue) is a climatic-influenced event; the four Greenland Interstadials (GI8-11) are all marked in the same color (green) for the sake of clarity.

5. Conclusions

The observation of CI fallout in Eifel maar lake sediments documents that the CI ash indeed reached Central Europe. The fallout occurred in the final decades of GI9, with

an age of 39,940 yr b2k ± 150 years. The CI indeed occurred between major changes in the Earth's environmental history (Laschamp geomagnetic excursion and Heinrich Event 4), but we do not see an immediate impact from the CI eruption itself. In general, the environmental impact in the Eifel was not strong; however, there were possible effects on local soil fertility and river runoff nutrient concentrations.

Author Contributions: Conceptualization: F.S. (Frank Sirocko), F.S. (Fiona Schenk) and U.H.; Methodology: F.S. (Fiona Schenk), F.S. (Frank Sirocko) and U.H.; Validation: U.H. and D.V.; Formal Analysis: F.S. (Fiona Schenk) and U.H.; Resources: F.S. (Frank Sirocko) and U.H.; Data Curation: F.S. (Fiona Schenk), F.S. (Frank Sirocko), U.H. and S.B.; Writing—Original Draft Preparation: F.S. (Fiona Schenk), U.H., S.B., D.V. and F.S. (Frank Sirocko); Funding Acquisition: F.S. (Frank Sirocko). All authors have read and agreed to the published version of the manuscript.

Funding: This research was funded by the Johannes Gutenberg University of Mainz.

Data Availability Statement: All data will be downloadable at the website of this project (https://elsa-project.de).

Acknowledgments: The authors thank Klaus Schwibus as well as Frank Dreher for the sampling and maintenance of the core repository, and Petra Sigl for the graphical design. Furthermore, the technical support at the Johannes Gutenberg University through the laboratory equipment by Stephan Buhre (EPMA) and Regina Mertz (LA-ICP-MS) is appreciated. The authors thank the team from the microprobe lab at the Bayerische GeoInstitut, namely, Anke Potzel and Detlef Kraußе, for their constant and crucial support during EPMA. We are particularly indebted to Raphael Njul for the careful and precise sample preparation. With great effort, Philipp Schulte and the team from the sedimentology lab of the Chair of Physical Geography and Geoecology of the RWTH Aachen University succeeded in isolating the heavy mineral fraction from the tephra at Urluia. We also thank the anonymous reviewers for their efforts and substantive comments, which contributed significantly to the improvement of the manuscript.

Conflicts of Interest: The authors declare no conflicts of interest.

Appendix A

Table A1. EPMA results of major elements (in mass percentage) of green single cpx minerals from Auel maar lake and Urluia outcrop compared to data from the Phlegraean Fields (only the most ubiquitous green cpxs of type Cpx2 from the data set of Fedele et al. [35]).

Sample ID	SiO_2	TiO_2	Al_2O_3	FeO	MnO	MgO	CaO	Na_2O
Auel (AU)								
AU-1	50.13	0.29	4.38	6.60	0.12	14.05	22.23	0.66
AU-2	49.54	0.63	3.76	8.37	0.39	13.20	22.60	0.43
AU-3	48.70	1.16	5.53	4.44	0.10	14.91	22.43	0.54
AU-4.2	49.87	0.65	2.57	8.90	0.78	12.84	22.15	0.64
Mean *	**49.56**	**0.68**	**4.06**	**7.08**	**0.35**	**13.75**	**22.35**	**0.57**
Urluia (URL)								
URL-1	49.10	0.54	3.47	8.11	0.44	13.23	22.55	0.43
URL-2	49.95	0.40	2.68	7.52	0.42	13.61	23.06	0.49
URL-4	48.17	0.71	4.05	8.51	0.41	12.80	22.69	0.48
URL-6.2	49.39	0.65	2.39	9.24	0.83	12.11	22.87	0.60
URL-6.3	49.53	0.82	3.98	6.33	0.36	14.31	22.36	0.45
Mean **	**49.23**	**0.63**	**3.31**	**8.00**	**0.49**	**13.21**	**22.71**	**0.49**
Phlegraean Fields, cf. Fedele et al. [35]								
Mean ***	**50.10**	**0.58**	**3.57**	**8.31**	**0.35**	**13.46**	**22.98**	**0.34**

* Mean AU, 4 samples; ** Mean URL, 5 samples; *** Mean Phlegraean Fields, 11 samples.

Table A2. (a) EPMA results of major elements (in mass percentage) of glass from Auel maar lake and Urluia outcrop compared to data from the Phlegraean Fields [35]. (b) EPMA results of major elements (in mass percentage) of glass from Auel maar lake and Urluia outcrop compared to data from the Phlegraean Fields [35].

(a)						
Sample ID	**Na_2O**	**K_2O**	**Cl**	**FeO**	**SiO_2**	**P_2O_5**
Urluia (URL)						
URL-3.2	8.88	5.18	0.59	3.52	55.27	0.00
URL-5	4.29	8.42	0.39	2.72	60.47	0.07
URL-6.1	4.68	8.02	0.51	3.04	58.03	0.04
URLb_4-3	6.04	7.60	0.64	2.76	59.26	0.06
URL_1-1a	4.18	8.47	0.35	2.99	60.12	0.10
Mean *	**5.61**	**7.54**	**0.50**	**3.01**	**58.63**	**0.05**
Auel **	**6.18**	**7.24**	**0.49**	**2.65**	**60.01**	**0.08**
Phlegraean Fields, cf. Fedele et al. [35]						
Mean ***	**4.53**	**8.42**		**2.84**	**59.78**	**0.20**
(b)						
Sample ID	**CaO**	**MnO**	**MgO**	**TiO_2**	**Al_2O_3**	**Total**
Urluia (URL)						
URL-3.2	1.30	0.42	0.19	0.35	22.51	98.21
URL-5	1.98	0.12	0.56	0.31	18.39	97.72
URL-6.1	2.07	0.18	0.58	0.44	17.87	95.46
URLb_4-3	1.73	0.24	0.33	0.42	18.43	97.50
URL_1-1a	2.12	0.10	0.52	0.35	18.03	97.33
Mean *	**1.84**	**0.21**	**0.44**	**0.37**	**19.05**	**97.25**
Auel **	**1.66**	**0.17**	**0.41**	**0.32**	**18.72**	**97.93**
Phlegraean Fields, cf. Fedele et al. [35]						
Mean ***	**1.96**	**0.22**	**0.47**	**0.38**	**18.18**	

* Mean Urluia, 5 points; ** Auel (AU-4.1, single point); *** Mean Phlegraean Fields, 38 samples.

Table A3. Average REE (in ppm and normalized to chondrite) compositions of cpx (LA-ICP-MS da-ta) for samples of type Cpx2 [35] from the Phlegraean Fields.

Element	**Mean Phlegraean Fields 11 Samples**	**Chondrite Normalized Data [51]**
La	16.18	66.16
Ce	54.09	84.80
Pr	9.82	101.88
Nd	54.82	115.70
Sm	16.22	105.31
Eu	4.68	80.71
Gd	15.32	74.98
Tb	2.05	54.86
Dy	12.25	48.19
Ho	2.08	36.75
Er	5.40	32.55
Tm	0.70	27.23
Yb	4.31	26.10
Lu	0.63	24.99

Table A4. Parts of elements in percentage from AU3 (69.60 m) compared to data from Urluia.

Oxides	Green Cpx (AU3, 69.60 m)	Green Cpx (Urluia)
Na_2O	0.33	0.65
SiO_2	45.52	50.98
K_2O	0.02	0.02
TiO_2	2.50	0.64
FeO	6.52	9.41
Al_2O_3	7.29	2.62
MgO	13.06	12.47
CaO	24.10	22.63
Cr_2O_3	0.14	0.07
MnO	0.10	0.74

Table A5. Measurements of REE [µg/g] from AU3 (69.60 m) compared to data from Urluia.

Element	Green Cpx (AU3, 69.60 m)	Green Cpx (Urluia)
La	51.39	53.31
Ce	67.97	73.85
Pr	70.77	86.54
Nd	67.60	93.42
Sm	43.96	82.34
Eu	34.06	68.42
Gd	24.87	57.81
Tb	15.03	44.94
Dy	12.40	38.65
Ho	8.55	29.10
Er	6.59	25.18
Tm	5.04	19.30
Yb	5.61	20.30
Lu	4.65	16.58

References

1. Sirocko, F.; Krebsbach, F.; Albert, J.; Britzius, S.; Schenk, F.; Förster, M.W. Relation between the Central European Climate Change and the Eifel Volcanism during the Last 130,000 Years: The ELSA-23 Tephra Stack. Preprints 2023, 2023121783. *Quaternary*, 2023; *submitted*.
2. Sirocko, F.; Martínez-García, A.; Mudelsee, M.; Albert, J.; Britzius, S.; Christl, M.; Diehl, D.; Diensberg, B.; Friedrich, R.; Fuhrmann, F.; et al. Muted Multidecadal Climate Variability in Central Europe during Cold Stadial Periods. *Nat. Geosci.* **2021**, *14*, 651–658. [CrossRef]
3. Förster, M.W.; Zemlitskaya, A.; Otter, L.M.; Buhre, S.; Sirocko, F. Late Pleistocene Eifel Eruptions: Insights from Clinopyroxene and Glass Geochemistry of Tephra Layers from Eifel Laminated Sediment Archive Sediment Cores. *J. Quat. Sci.* **2020**, *35*, 186–198. [CrossRef]
4. Silleni, A.; Giordano, G.; Isaia, R.; Ort, M.H. The Magnitude of the 39.8 ka Campanian Ignimbrite Eruption, Italy: Method, Uncertainties and Errors. *Front. Earth Sci.* **2020**, *8*, 543399. [CrossRef]
5. Pabst, S.; Wörner, G.; Civetta, L.; Tesoro, R. Magma Chamber Evolution Prior to the Campanian Ignimbrite and Neapolitan Yellow Tuff Eruptions (Campi Flegrei, Italy). *Bull. Volcanol.* **2008**, *70*, 961–976. [CrossRef]
6. Fisher, R.V.; Schmincke, H.-U. *Pyroclastic Rocks*; Springer: Berlin/Heidelberg, Germany, 1984; ISBN 978-3-540-12756-7.
7. Fedele, F.G.; Giaccio, B.; Isaia, R.; Orsi, G. The Campanian Ignimbrite Eruption, Heinrich Event 4, and Palaeolithic Change in Europe: A High-Resolution Investigation. *Geophys. Monogr. Ser.* **2003**, *139*, 301–325. [CrossRef]
8. Thunell, R.; Federman, A.; Sparks, S.; Williams, D. The Age, Origin, and Volcanological Significance of the Y-5 Ash Layer in the Mediterranean. *Quat. Res.* **1979**, *12*, 241–253. [CrossRef]
9. De Vivo, B.; Rolandi, G.; Gans, P.B.; Calvert, A.; Bohrson, W.A.; Spera, F.J.; Belkin, H.E. New Constraints on the Pyroclastic Eruptive History of the Campanian Volcanic Plain (Italy). *Mineral. Petrol.* **2001**, *73*, 47–65. [CrossRef]
10. Giaccio, B.; Hajdas, I.; Isaia, R.; Deino, A.; Nomade, S. High-Precision ^{14}C and $^{40}Ar/^{39}Ar$ Dating of the Campanian Ignimbrite (Y-5) Reconciles the Time-Scales of Climatic-Cultural Processes at 40 ka. *Sci. Rep.* **2017**, *7*, 45940. [CrossRef]
11. Lin, J.; Svensson, A.; Hvidberg, C.S.; Lohmann, J.; Kristiansen, S.; Dahl-Jensen, D.; Steffensen, J.P.; Rasmussen, S.O.; Cook, E.; Kjær, H.A.; et al. Magnitude, Frequency and Climate Forcing of Global Volcanism during the Last Glacial Period as Seen in Greenland and Antarctic Ice Cores (60–9 ka). *Clim. Past* **2022**, *18*, 485–506. [CrossRef]

12. Paterne, M.; Kallel, N.; Labeyrie, L.; Vautravers, M.; Duplessy, J.; Rossignol-Strick, M.; Cortijo, E.; Arnold, M.; Fontugne, M. Hydrological Relationship between the North Atlantic Ocean and the Mediterranean Sea during the Past 15–75 kyr. *Paleoceanography* **1999**, *14*, 626–638. [CrossRef]
13. Ton-That, T.; Singer, B.; Paterne, M. $^{40}Ar/^{39}Ar$ Dating of Latest Pleistocene (41 ka) Marine Tephra in the Mediterranean Sea: Implications for Global Climate Records. *Earth Planet. Sci. Lett.* **2001**, *184*, 645–658. [CrossRef]
14. Veres, D.; Lane, C.S.; Timar-Gabor, A.; Hambach, U.; Constantin, D.; Szakács, A.; Fülling, A.; Onac, B.P. The Campanian Ignimbrite/Y5 Tephra Layer—A Regional Stratigraphic Marker for Isotope Stage 3 Deposits in the Lower Danube Region, Romania. *Quat. Int.* **2013**, *293*, 22–33. [CrossRef]
15. Giaccio, B.; Isaia, R.; Fedele, F.G.; Di Canzio, E.; Hoffecker, J.; Ronchitelli, A.; Sinitsyn, A.A.; Anikovich, M.; Lisitsyn, S.N.; Popov, V.V. The Campanian Ignimbrite and Codola Tephra Layers: Two Temporal/Stratigraphic Markers for the Early Upper Palaeolithic in Southern Italy and Eastern Europe. *J. Volcanol. Geotherm. Res.* **2008**, *177*, 208–226. [CrossRef]
16. Narcisi, B. Tephrochronology of a Late Quaternary Lacustrine Record from the Monticchio Maar (Vulture Volcano, Southern Italy). *Quat. Sci. Rev.* **1996**, *15*, 155–165. [CrossRef]
17. Keller, J.; Ryan, W.B.F.; Ninkovich, D.; Altherr, R. Explosive Volcanic Activity in the Mediterranean over the Past 200,000 yr as Recorded in Deep-Sea Sediments. *Geol. Soc. Am. Bull.* **1978**, *89*, 591–604. [CrossRef]
18. Fedele, L.; Scarpati, C.; Sparice, D.; Perrotta, A.; Laiena, F. A Chemostratigraphic Study of the Campanian Ignimbrite Eruption (Campi Flegrei, Italy): Insights on Magma Chamber Withdrawal and Deposit Accumulation as Revealed by Compositionally Zoned Stratigraphic and Facies Framework. *J. Volcanol. Geotherm. Res.* **2016**, *324*, 105–117. [CrossRef]
19. Scarpati, C.; Perrotta, A. Stratigraphy and Physical Parameters of the Plinian Phase of the Campanian Ignimbrite Eruption. *Geol. Soc. Am. Bull.* **2016**, *128*, 1147–1159. [CrossRef]
20. Smith, V.C.; Isaia, R.; Engwell, S.L.; Albert, P.G. Tephra Dispersal during the Campanian Ignimbrite (Italy) Eruption: Implications for Ultra-Distal Ash Transport during the Large Caldera-Forming Eruption. *Bull. Volcanol.* **2016**, *78*, 45. [CrossRef]
21. Civetta, L.; Orsi, G.; Pappalardo, L.; Fisher, R.V.; Heiken, G.; Ort, M. Geochemical Zoning, Mingling, Eruptive Dynamics and Depositional Processes—The Campanian Ignimbrite, Campi Flegrei Caldera, Italy. *J. Volcanol. Geotherm. Res.* **1997**, *75*, 183–219. [CrossRef]
22. Engwell, S.L.; Sparks, R.S.J.; Carey, S. Physical Characteristics of Tephra Layers in the Deep Sea Realm: The Campanian Ignimbrite Eruption. *Geol. Soc. Lond. Spec. Publ.* **2014**, *398*, 47–64. [CrossRef]
23. Fedele, F.G.; Giaccio, B.; Hajdas, I. Timescales and Cultural Process at 40,000 BP in the Light of the Campanian Ignimbrite Eruption, Western Eurasia. *J. Hum. Evol.* **2008**, *55*, 834–857. [CrossRef] [PubMed]
24. Fitzsimmons, K.E.; Hambach, U.; Veres, D.; Iovita, R. The Campanian Ignimbrite Eruption: New Data on Volcanic Ash Dispersal and Its Potential Impact on Human Evolution. *PLoS ONE* **2013**, *8*, e65839. [CrossRef] [PubMed]
25. Nowaczyk, N.R.; Arz, H.W.; Frank, U.; Kind, J.; Plessen, B. Dynamics of the Laschamp Geomagnetic Excursion from Black Sea Sediments. *Earth Planet. Sci. Lett.* **2012**, *351–352*, 54–69. [CrossRef]
26. Wacha, L.; Mikulčić Pavlaković, S.; Frechen, M.; Crnjaković, M. The loess chronology of the Island of Susak, Croatia. *EG Quat. Sci. J.* **2011**, *60*, 153–169. [CrossRef]
27. Tsanova, T.; Veres, D.; Hambach, U.; Spasov, R.; Dimitrova, I.; Popov, P.; Talamo, S.; Sirakova, S. Upper Palaeolithic Layers and Campanian Ignimbrite/Y-5 Tephra in Toplitsa Cave, Northern Bulgaria. *J. Archaeol. Sci. Rep.* **2021**, *37*, 102912. [CrossRef]
28. Masotta, M.; Mollo, S.; Freda, C.; Gaeta, M.; Moore, G. Clinopyroxene–Liquid Thermometers and Barometers Specific to Alkaline Differentiated Magmas. *Contrib. Mineral. Petrol.* **2013**, *166*, 1545–1561. [CrossRef]
29. Tomlinson, E.L.; Smith, V.C.; Albert, P.G.; Aydar, E.; Civetta, L.; Cioni, R.; Çubukçu, E.; Gertisser, R.; Isaia, R.; Menzies, M.A.; et al. The Major and Trace Element Glass Compositions of the Productive Mediterranean Volcanic Sources: Tools for Correlating Distal Tephra Layers in and around Europe. *Quat. Sci. Rev.* **2015**, *118*, 48–66. [CrossRef]
30. Obreht, I.; Hambach, U.; Veres, D.; Zeeden, C.; Bösken, J.; Stevens, T.; Marković, S.B.; Klasen, N.; Brill, D.; Burow, C.; et al. Shift of Large-Scale Atmospheric Systems over Europe during Late MIS 3 and Implications for Modern Human Dispersal. *Sci. Rep.* **2017**, *7*, 5848. [CrossRef] [PubMed]
31. Marković, S.B.; Stevens, T.; Kukla, G.J.; Hambach, U.; Fitzsimmons, K.E.; Gibbard, P.; Buggle, B.; Zech, M.; Guo, Z.; Hao, Q.; et al. Danube Loess Stratigraphy—Towards a Pan-European Loess Stratigraphic Model. *Earth Sci. Rev.* **2015**, *148*, 228–258. [CrossRef]
32. Deino, A.L.; Orsi, G.; De Vita, S.; Piochi, M. The Age of the Neapolitan Yellow Tuff Caldera-Forming Eruption (Campi Flegrei Caldera—Italy) Assessed by $^{40}Ar/^{39}Ar$ Dating Method. *J. Volcanol. Geotherm. Res.* **2004**, *133*, 157–170. [CrossRef]
33. Schmidt, R.; Van Den Bogaard, C.; Merkt, J.; Müller, J. A New Lateglacial Chronostratigraphic Tephra Marker for the South-Eastern Alps: The Neapolitan Yellow Tuff (NYT) in Längsee (Austria) in the Context of a Regional Biostratigraphy and Palaeoclimate. *Quat. Int.* **2002**, *88*, 45–56. [CrossRef]
34. Lenaz, D.; Marciano, R.; Veres, D.; Dietrich, S.; Sirocko, F. Mineralogy of the Dehner and Jungferweiher Maar Tephras (Eifel, Germany). *Neues Jahrb. Geol. Paläontol. Abh. Band* **2010**, *257*, 55–67. [CrossRef]
35. Fedele, L.; Zanetti, A.; Morra, V.; Lustrino, M.; Melluso, L.; Vannucci, R. Clinopyroxene/Liquid Trace Element Partitioning in Natural Trachyte–Trachyphonolite Systems: Insights from Campi Flegrei (Southern Italy). *Contrib. Mineral. Petrol.* **2009**, *158*, 337–356. [CrossRef]
36. Kendrick, J. Strain Localisation during Dome-Building Eruptions. Ph.D. Thesis, Ludwig-Maximilians-Universität (LMU), Munich, Germany, 2013.

37. Reed, S.J.B. *Electron Microprobe Analysis and Scanning Electron Microscopy in Geology*, 2nd ed.; Camebridge University Press: Camebridge, UK, 2005; ISBN 978-0-511-61056-1.
38. Prelević, D.; Akal, C.; Romer, R.L.; Mertz-Kraus, R.; Helvac, C. Magmatic Response to Slab Tearing: Constraints from the Afyon Alkaline Volcanic Complex, Western Turkey. *J. Petrol.* **2015**, *56*, 527–562. [CrossRef]
39. Günther, D.; Frischknecht, R.; Heinrich, C.A.; Kahlert, H.-J. Capabilities of an Argon Fluoride 193 Nm Excimer Laser for Laser Ablation Inductively Coupled Plasma Mass Spectometry Microanalysis of Geological Materials. *J. Anal. At. Spectrom.* **1997**, *12*, 939–944. [CrossRef]
40. Jochum, K.P.; Weis, U.; Stoll, B.; Kuzmin, D.; Yang, Q.; Raczek, I.; Jacob, D.E.; Stracke, A.; Birbaum, K.; Frick, D.A.; et al. Determination of Reference Values for NIST SRM 610–617 Glasses Following ISO Guidelines. *Geostand. Geoanalyt. Res.* **2011**, *35*, 397–429. [CrossRef]
41. Longerich, H.P.; Jackson, S.E.; Günther, D. Inter-Laboratory Note. Laser Ablation Inductively Coupled Plasma Mass Spectrometric Transient Signal Data Acquisition and Analyte Concentration Calculation. *J. Anal. At. Spectrom.* **1996**, *11*, 899–904. [CrossRef]
42. Richter, T.O.; Van Der Gaast, S.; Koster, B.; Vaars, A.; Gieles, R.; De Stigter, H.C.; De Haas, H.; Van Weering, T.C.E. The Avaatech XRF Core Scanner: Technical Description and Applications to NE Atlantic Sediments. *Geol. Soc. Lond. Spec. Publ.* **2006**, *267*, 39–50. [CrossRef]
43. Berglund, B.E.; Ralska-Jasiewiczowa, M. Pollen Analysis and Pollen Diagrams. In *Handbook of Holocene Palaeoecology and Palaeohydrology*; Berglund, B.E., Ed.; John Wiley and Sons: Chichester, UK, 1986; Volume 19, pp. 455–484. ISBN 978-0-471-90691-9.
44. Fægri, K.; Iversen, J. *Textbook of Pollen Analysis*, 4th ed.; Joahn Wiley & Sons: Chichester, UK, 1989; ISBN 978-0-471-92178-3.
45. Britzius, S.; Dreher, F.; Maisel, P.; Sirocko, F. Vegetation Patterns during the Last 132,000 Years: A Synthesis from Twelve Eifel Maar Sediment Cores (Germany): The ELSA-23-Pollen-Stack. *Quaternary* **2024**, *7*, 8. [CrossRef]
46. Kendrick, J.E.; Lavallée, Y.; Mariani, E.; Dingwell, D.B.; Wheeler, J.; Varley, N.R. Crystal Plasticity as an Indicator of the Viscous-Brittle Transition in Magmas. *Nat. Commun.* **2017**, *8*, 1926. [CrossRef]
47. Okumura, S.; Kushnir, A.R.L.; Martel, C.; Champallier, R.; Thibault, Q.; Takeuchi, S. Rheology of Crystal-Bearing Natural Magmas: Torsional Deformation Experiments at 800 °C and 100 MPa. *J. Volcanol. Geotherm. Res.* **2016**, *328*, 237–246. [CrossRef]
48. Holness, M.B.; Stock, M.J.; Geist, D. Magma Chambers versus Mush Zones: Constraining the Architecture of Sub-Volcanic Plumbing Systems from Microstructural Analysis of Crystalline Enclaves. *Phil. Trans. R. Soc. A* **2019**, *377*, 20180006. [CrossRef] [PubMed]
49. Arbaret, L.; Bystricky, M.; Champallier, R. Microstructures and Rheology of Hydrous Synthetic Magmatic Suspensions Deformed in Torsion at High Pressure. *J. Geophys. Res.* **2007**, *112*, B10208. [CrossRef]
50. Wulf, S.; Hardiman, M.J.; Staff, R.A.; Koutsodendris, A.; Appelt, O.; Blockley, S.P.E.; Lowe, J.J.; Manning, C.J.; Ottolini, L.; Schmitt, A.K.; et al. The Marine Isotope Stage 1–5 Cryptotephra Record of Tenaghi Philippon, Greece: Towards a Detailed Tephrostratigraphic Framework for the Eastern Mediterranean Region. *Quat. Sci. Rev.* **2018**, *186*, 236–262. [CrossRef]
51. Evensen, N.M.; Hamilton, P.J.; O'Nions, R.K. Rare-Earth Abundances in Chondritic Meteorites. *Geochim. Cosmochim. Acta* **1978**, *42*, 1199–1212. [CrossRef]
52. Fedele, L.; Scarpati, C.; Lanphere, M.; Melluso, L.; Morra, V.; Perrotta, A.; Ricci, G. The Breccia Museo Formation, Campi Flegrei, Southern Italy: Geochronology, Chemostratigraphy and Relationship with the Campanian Ignimbrite Eruption. *Bull. Volcanol.* **2008**, *70*, 1189–1219. [CrossRef]
53. Rasmussen, S.O.; Bigler, M.; Blockley, S.P.; Blunier, T.; Buchardt, S.L.; Clausen, H.B.; Cvijanovic, I.; Dahl-Jensen, D.; Johnsen, S.J.; Fischer, H.; et al. A Stratigraphic Framework for Abrupt Climatic Changes during the Last Glacial Period Based on Three Synchronized Greenland Ice-Core Records: Refining and Extending the INTIMATE Event Stratigraphy. *Quat. Sci. Rev.* **2014**, *106*, 14–28. [CrossRef]
54. Costa, A.; Folch, A.; Macedonio, G.; Giaccio, B.; Isaia, R.; Smith, V.C. Quantifying Volcanic Ash Dispersal and Impact of the Campanian Ignimbrite Super-eruption. *Geophys. Res. Lett.* **2012**, *39*, 2012GL051605. [CrossRef]
55. Martrat, B.; Grimalt, J.O.; Shackleton, N.J.; de Abreu, L.; Hutterli, M.A.; Stocker, T.F. Four Climate Cycles of Recurring Deep and Surface Water Destabilizations on the Iberian Margin. *Science* **2007**, *317*, 502–507. [CrossRef]
56. Berger, A.; Loutre, M.F. Insolation Values for the Climate of the Last 10 Million Years. *Quat. Sci. Rev.* **1991**, *10*, 297–317. [CrossRef]
57. Korte, M.; Brown, M.C.; Panovska, S.; Wardinski, I. Robust Characteristics of the Laschamp and Mono Lake Geomagnetic Excursions: Results From Global Field Models. *Front. Earth Sci.* **2019**, *7*, 86. [CrossRef]
58. Muscheler, R.; Beer, J.; Kubik, P.W.; Synal, H.-A. Geomagnetic Field Intensity during the Last 60,000 Years Based on ^{10}Be and ^{36}Cl from the Summit Ice Cores and ^{14}C. *Quat. Sci. Rev.* **2005**, *24*, 1849–1860. [CrossRef]
59. Albert, J.; Sirocko, F. Evidence for an Extreme Cooling Event Prior to the Laschamp Geomagnetic Excursion in Eifel Maar Sediments. *Quaternary* **2023**, *6*, 14. [CrossRef]